**Eleventh U.S. National Conference on Earthquake Engineering**
*Integrating Science, Engineering & Policy*
June 25-29, 2018
Los Angeles, California

# NONLINEAR BODY WAVES IN THE SHALLOW SUBSURFACE, IMPLICATIONS OF FLOW-LAW RHEOLOGIES

Norman H. Sleep[1] and Nori Nakata[2]

## ABSTRACT

Major earthquakes produce high-frequency body waves that impinge over extended periods of time. These waves refract into nearly vertical paths in the low-velocity shallow subsurface. Scaling relationships of laterally homogeneous models for exactly vertical waves illustrate features that arise in fully three-dimensional numerical models and the real Earth. Flow-law rheologies yield testable hypotheses, especially when different types of seismic waves interact. S-waves produce horizontal shear tractions on horizontal surfaces. The anelastic strain rate depends nonlinearly on the horizontal shear traction. The horizontal shear traction is the product of the shear modulus times the difference between total strain and anelastic strain. Damage where anelastic strain decreases the shear modulus and the shear modulus heals after shaking is finished can also be included. Anelastic strain continues when the material is driven at constant stress and stresses relax at constant strain. In contrast, the widely used Masing rules make the counter-intuitive prediction that no further strain occurs in when the material is maintained at constant stress. Conveniently, natural experiments allow appraisal. The Coulomb ratio of dynamic to lithostatic stress is approximately the dynamic (resolved horizontal) acceleration in g's. The anelastic strain rate for frictional materials increases rapidly with shear traction. The resolved peak horizontal acceleration (peak ground acceleration, PGA) of *S* waves thus clips in g's at the effective coefficient of friction. Strong tensional *P* waves then suppress *S* waves. Anelastic strain commences at low stresses for muddy soils, but increases slowly with stress. Nonlinear attenuation increases slowly at high shear tractions. Accelerations over 1 g can occur, especially when waves reverberate with the shallow layer. *P* waves have little effect. That is, the rheology is nonlinear viscous not Coulomb. Records from the Kumamoto 2016 strong earthquakes from KIK-net station KMMH16 display the expected effects for drained muddy soil. Reverberating *S* waves should interact with shallow distributed slip above the fault trace.

[1]Professor, Dept. of Geophysics, Stanford. University, Stanford, CA 94025 (email: norm@stanford.edu)
[2]Assistant Professor, School of Geology and Geophysics, University of Oklahoma, Norman, OK 73019

Sleep NH, Nakata N. Nonlinear body waves in the shallow subsurface, implications of flow-law rheologies. *Proceedings of the 11th National Conference in Earthquake Engineering*, Earthquake Engineering Research Institute, Los Angeles, CA. 2018.

# Nonlinear body waves in the shallow subsurface, implications of flow-law rheologies

Norman H. Sleep[1] and Nori Nakata[2]

## ABSTRACT

Major earthquakes produce high-frequency body waves that impinge over extended periods of time. These waves refract into nearly vertical paths in the low-velocity shallow subsurface. caling relationships of laterally homogeneous models for exactly vertical waves illustrate features that arise in fully three-dimensional numerical models and the real Earth. Flow-law rheologies yield testable hypotheses, especially when different types of seismic waves interact. S-waves produce horizontal shear tractions on horizontal surfaces. The anelastic strain rate depends nonlinearly on the horizontal shear traction. The horizontal shear traction is the product of the shear modulus times the difference between total strain and anelastic strain. Damage where anelastic strain decreases the shear modulus and the shear modulus heals after shaking is finished can also be included. Anelastic strain continues when the material is driven at constant stress and stresses relax at constant strain. In contrast, the widely used Masing rules make the counter-intuitive prediction that no further strain occurs in when the material is maintained at constant stress. Conveniently, natural experiments allow appraisal. The Coulomb ratio of dynamic to lithostatic stress is approximately the dynamic (resolved horizontal) acceleration in g's. The anelastic strain rate for frictional materials increases rapidly with shear traction. The resolved peak horizontal acceleration (peak ground acceleration, PGA) of *S* waves thus clips in g's at the effective coefficient of friction. Strong tensional *P* waves then suppress *S* waves. Anelastic strain commences at low stresses for muddy soils, but increases slowly with stress. Nonlinear attenuation increases slowly at high shear tractions. Accelerations over 1 g can occur, especially when waves reverberate with the shallow layer. *P* waves have little effect. That is, the rheology is nonlinear viscous not Coulomb. Records from the Kumamoto 2016 strong earthquakes from KIK-net station KMMH16 display the expected effects for drained muddy soil. Reverberating *S* waves should interact with shallow distributed slip above the fault trace.

## Introduction

Dynamic stresses from strong seismic waves impinge on the shallow subsurface, sometimes bringing rocks and soils beyond their elastic limits. Anelastic failure damages the material reducing its shear modulus. Anelastic deformation also dissipates energy from the waves, reducing the overall amplitude of shaking at the surface. Strong surface waves may produce nonlinear failure anywhere along their paths. Site-response formalism is then inappropriate. We hence concentrate on effects related to body waves, where empirical site responses already provide some insight. Our task is to provide and appraise the physical bases for site response. We begin with a general discussion of flow laws, as they have not been widely applied to shallow nonlinear seismology. We then discuss the three-dimensional interaction of different types of seismic waves to provide insight into rheology. We then discuss interaction of strong *S* waves

[1] Professor, Dept. of Geophysics, Stanford. University, Stanford, CA 94025 (email: norm@stanford.edu)
[2] Assistant Professor, School of Geology and Geophysics, University of Oklahoma, Norman, OK 73019

Sleep NH, Nakata N. Nonlinear body waves in the shallow subsurface, implications of flow-law rheologies. *Proceedings of the 11th National Conference in Earthquake Engineering*, Earthquake Engineering Research Institute, Los Angeles, CA. 2018.

with strong *P* waves with regard to the behavior of muddy soils and interaction of shallow distributed fault slip with strong *S* waves as applications.

## Flow Laws for Shallow Rocks and Soil

It is necessary to infer the mechanical properties including failure rheology of the shallow subsurface to obtain scaling relationships and implement numerical models. We begin with vertically propagating *S* waves for simplicity. These waves produce dynamic shear tractions $\tau_{xz}$ and $\tau_{xy}$ (where $x$ and $y$ are horizontal coordinates and $z$ is depth) on horizontal planes. A flow-law rheology is attractive for both frictional rock and viscous mud. Formally, the anelastic strain rate (vertically distributed shear on horizontal planes) is

$$\dot{\varepsilon}_{iz} = \left(\frac{\tau_{iz}}{|\tau|}\right) F\left(|\tau|, P_N\right), \tag{1}$$

where $|\tau|$ is the resolved horizontal shear traction, $i$ is a horizontal tensor index, the first bracket indicates that shearing has the orientation of the applied shear traction, $F$ is a function with dimensions of strain rate that may be strongly nonlinear, and $P_N$ is the compressional normal traction on the horizontal plane. The shear traction in term is proportional to the difference between total strain $e_{iz}$ and anelastic strain $\varepsilon_{iz}$,

$$\tau_{iz} = 2G(e_{iz} - \varepsilon_{iz}), \tag{2}$$

where $G$ is the shear modulus. For frictional rheology, the anelastic strain rate increases from very slow to very fast when $|\tau| = \mu P_N$, where $\mu$ is the coefficient of friction.

The anelastic strain rate may cause damage that reduces the shear modulus,

$$\frac{\partial G}{\partial t} = -C_1|\dot{\varepsilon}| + C_2(G_0 - G)^N, \tag{3}$$

where $C_1$ is material property that represents damage, $|\dot{\varepsilon}|$ is the resolved anelastic strain rate, $C_2$ is a material property related to healing, $N > 1$ is an exponent, and the shear modulus in the absence of shaking eventually heals toward $G_0$.

Flow laws readily extend to three dimensions. One needs to keep track of the total strain $\varepsilon_{ij}$ (where $i$ and $j$ are any tensor indices) using numerical displacements, anelastic strain $\varepsilon_{ij}$, and (if damage is present) changes in $G$ to evaluate stress. One need not to numerically keep track of past history beyond that needed to include acceleration in the wave equation. Existing nonlinear numerical models of seismic waves include flow laws to represent plastic material where the anelastic strain rate increases from extremely small to extremely fast when a frictional yield stress is reached [1-2]. Geodynamists traditionally apply flow laws to represent mantle convection. Flow laws have the attractive mantle-convection attribute that a viscous material continues to creep anelastically when driven constant deviatoric stress.

Flow laws, however, have not been widely used to represent shallow rock and soil failure. Rather traditionally, one relates total strain $e$ (for brevity with scalars for a vertical *S* wave with motion in one direction) to stress $\tau$ (Figure 1). At small strains, the material is elastic and $\tau = G_{\text{int}}\varepsilon$, where $G_{\text{int}}$ is the initial elastic shear modulus. The differential shear modulus

$G_{diff} = \partial\tau / \partial e$ decreases below the elastic one as total strain increases. When the sense of the change shear or shear reverses $G_{diff}$ returns to $G_{int}$. Attenuation is proportional to the area of the loop. Masing rules keep track of $G_{diff}$ over complicated deformation paths when extended to three dimensions [3] and to frictional rheology [4]. Furthermore, Masing rules and flow laws predict behavior qualitatively similar behavior when material is driven back and forth repeated between the same end strains (here points A and B). Differences become evident when material is driven in a complicated manner [5]. A flow-law material approaches elastic behavior if driven at high frequency, while the stress-strain loop for Masing rules does not depend on frequency.

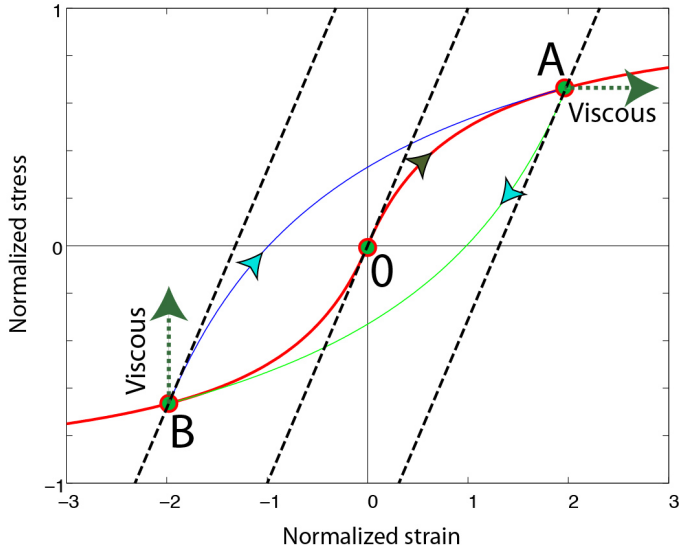


Figure 1. A stress-strain history illustrates the implications of Masing rules. The material starts at zero stress and strain and deforms elastically along the dashed line. The slope of the curve decreases with strain. The initial slope at the strain reversal at point A is parallel to the initial elastic slope at 0. Stress and strain then follow path through A and B over repeated cycles. The formulation has the testable unattractive features that the path has not depend on the driving frequency and that no further strain occurs if the material is held at high stress. A viscous material continues to accumulate strain if the material is held at constant stress, say at point A. The stress relaxes slowly if it is held at constant strain, say at point B.

## Natural Experiments for Physics-based Modeling

Soil and rock rheologies are not obvious in three dimensions. Basically, one may consider tractions resolved on oriented cracks with frictional a rheology. Failure occurs when the resolved shear traction $\tau$ exceeds a failure criterion $\tau > \mu P_N$, where $\mu$ is the coefficient of friction and $P_N$ is the normal traction. This (simple-shear) rheology is attractive for vertically propagating *S* waves crossing horizontal bedding planes. Alternatively, more may consider a pervasively cracked rock or a massive soil to be a continuum with internal friction. A Drucker-Prager type rheology [6] represents this behavior. A simple failure criterion is $|\tau| > \mu |P|$, where $|\tau| \propto \sqrt{\tau_{ij}\tau_{ij}}$ is

the second invariant of the deviatoric stress tensor normalized so that it gives the simple-shear result, and $|P| = -\sigma_{ii}/3$ is the mean stress compression positive. In addition, it is well known that the slip rate on frictional surfaces (and the strain rate within fault gouge) increases from very slow to very fast over a finite range of stress, rather than being perfectly plastic. The formalism of rate and state friction [7-8] models this behavior including the dependence on past slip. In terms of equation (1), the strain rate increases very rapidly with deviatoric stress and shear traction when the failure criterion is approached as:

$$\dot{\varepsilon}_{ij} = \left(\frac{\tau_{ij}}{|\tau|}\right) F\left(|\tau|/|P|\right). \tag{4}$$

This formalism may apply to cracked hard rock, exhumed sediments, and gravel where frictional contacts between hard grains exist. In contrast, the strain rate within a muddy soil may be that of a nonlinear viscous material and depends weakly on the mean stress. The strain rate increases nonlinearly but gradually over a wide range of $|\tau|$, the deviatoric stress invariant.

In our previous studies, we have shown that the interaction of different types of seismic waves provides natural experiments that constrain rheology [9-11]. We appraise whether different components of the deviatoric stress tensor interact through the invariant $|\tau|$ as expected from Eq. 4 and whether changes in mean stress and normal traction on horizontal planes affect the aneastic strain rate. For example, nonlinear attenuation of strong vertically propagating high-frequency *S* waves involves anelastic shear along horizontal planes. Strong longer period Love waves increase $|\tau|$ by putting horizontal shear traction on vertical planes. Strong longer period Rayleigh waves increase $|\tau|$ by increasing the difference between the horizontal stress in their propagating direction and the vertical stress that does not change much. Both of these effects increase the rate of anelastic deformation driven by *S* waves and hence suppress these waves. As example applications, we consider nonlinear interaction of strong *S* waves with strong *P* waves in viscous muddy soil and compare it with the expected behavior of a frictional material. We also consider the interaction of strong reverberating *S* waves with distributed near-fault deformation above a strike-slip in a muddy soil as examples with different components of the deviatoric stress tensor.

## Nonlinear Attenuation within a Muddy Soil

We discuss records from Kumamoto main shock (USGS $M_w$=7.0: 2016-04-15 16:25:06 UTC) to illustrate the behavior of viscous soil versus cracked rock with frictional rheology. We begin with well-known scaling relationships for shallow shear tractions for vertically propagating body waves. The shear traction is zero at the free surface. The normal traction does not change significantly. At the dominant frequency in broadband signal, the dynamic (resolved horizontal) shear traction increases linearly downward as $|\tau| \sim A\rho z$, where $A_S$ is dynamic acceleration due to *S*-waves and $z$ is depth. The lithostatic stress increases as $P_N \sim \rho g z$. We ignore fluid pressure for brevity and with forethought to our data. The Coulomb failure criterion becomes

$$\left|\frac{\tau}{P_N}\right| = \mu \sim \frac{A_S}{g}. \tag{5}$$

That is, frictional failure occurs when the normalized dynamic acceleration (in g's) equals the coefficient of friction. Thus, the effective coefficient of friction bounds (or clips) a long sequence of strong *S* waves at the same normalized acceleration (i.e., \mu g). This effect would be evident in sufficient long episode of shaking. A frequency-domain approach would obscure this relationship.

A homologous result applies to *P* waves with the understanding that downward acceleration produces dynamic tension. This effect results in a well-known asymmetry in dynamic failure from *P* waves [12-16]. Cracked rocks are weak and tension. Absolute tension occurs at freefall with a downward dynamic acceleration of 1 g. Downward accelerations exceeding 1 g are thus rare. Conversely, rocks are strong in compression and upward dynamic accelerations exceeding 1 g are common.

The tensional dynamic stresses from strong *P* waves thus should suppress strong *S* waves. The criterion in Eq. 5 becomes

$$\left[\frac{A_S}{g}\right] < \mu + \mu_{\text{diff}}\left[\frac{A_P}{g}\right], \tag{6}$$

where $A_P$ is the dynamic acceleration (upward positive) from *P* waves and the differential coefficient of friction for changes in normal traction $\mu_{\text{diff}}$ may be less than the ambient one $\mu$. Absolute downward accelerations approaching 1 g are thus expected to strongly suppress *S* waves. Tobita et al. [14] examined records from station IWTH25 above the hypocenter of the 2008 Iwate-Miyagi earthquake for this effect. They found that *S* waves were in fact suppressed, but that some *S*-wave energy still leaked to the surface while strong tensional *P* waves were present. Interlocking structure of cracks came into tension but supported some horizontal shear traction.

Proceeding to data from the Kumamoto main shock, co-located surface and borehole seismographs recorded strong shaking at KiK-net station KMMH16 (32.7933°N, 130.822°E), which is the closest KiK-net station to the epicenter. Goto et al. [17] studied reverberations within a shallow clay-rich soil formed on pyroclastic deposits and obtained an improved shallow low-amplitude *S*-wave structure from that provided by the National Research Institute for Earth Science and Disaster Resilience. The uppermost layer is 3 m thick and has a velocity ~80 m/s and the velocity between 3 to 9 m is ~130 m/s overlies ~350 m/s rocks. Resonance occurs over a ranges with peaks at ~5 Hz and ~3.5 Hz. The water table is beneath the resonant layer.

The mainshock produced mainly NW-SE *S*-wave motion at the borehole and surface stations [17]. The resonant frequencies decreased during strong shaking indicating that dynamic stresses damaged the layer. Damage started at low dynamic acceleration of 0.1-0.2 g [17], which is appropriate for viscous mud. However, the resolved acceleration and the SE acceleration reached 1.5 g, which may be appropriate for viscous clay. From Eq. 5, a coefficient of friction of ~1.5 would not be expected for clay-poor frictional rock.

The *P* waves during the strong *S* wave (Figure 2) were too feeble to provide a good test of Eq. 6. They do serve to illustrate the kinematics. The *P* wave velocity in the resonating layer was greater than the *S* wave velocity as expected. Multiple *P* wave cycles occurred during the strong *S* wave excursion. The signal is reasonably broadband as opposed to monochromatic; so propagating waves provide some insight. The upgoing and downgoing *P* waves overtake *S*

waves. The stronger *S* amplitudes would have encountered strong tensional *P* waves had they been present. The overall effect is that strong *P* waves suppress strong *S* waves. Once attenuated *S* waves do not regain strength during the compression cycle of the *P* waves. Eq. 6 provides guidance on nonlinear attenuation of *S* waves from the tension cycle within a frictional material.

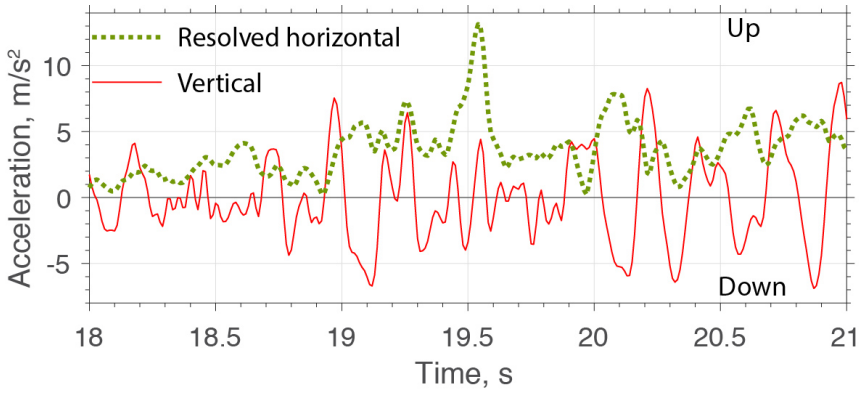


Figure 2. Resolved horizontal acceleration at surface station KMMH16 for the Kumamoto main shock. *S* waves and *P* waves reverberated within a shallow layer. Multiple *P* waves cycles occurred during the strongest *S*-wave excursion.

## Finite Width of Surface Rupture

Earthquakes sometimes rupture to the surface with knife-edge fault planes, but this is not always the case [18]. Broad zones of shallow rupture damage human structures but they do not affect the hazard associated with strong off-fault seismic waves. They do provide evidence for nonlinear interaction of body waves and the rupture tip in shallow subsurface. We point out that distributed fault deformation occurred in the Kumamoto mainshock [19] and foreshock [20]. We present a generic nonlinear model for this phenomenon.

We consider a strike-slip fault for simplicity. The earthquake begins in hard rocks and rupture eventually reaches low-velocity sediments and rocks in the shallow subsurface (Figure 3). The rupture propagation velocity (vector in fault plane perpendicular to the rupture front) scales with the local *S* wave velocity. Shallow rupture propagation thus refracts into a nearly vertical path. That is, the shallow rupture front is essentially mode 3.

There is opportunity for high-frequency *S* waves to interact with the very shallow rupture tip. The *S* waves typically reach the surface before the rupture tip. They continue to arrive for an extended period of time from the large fault surface. Shallow slip takes a finite time, 2-3 s for near-fault stations 93048 and 93051 for the Kumamoto mainshock [21].

The stress and strain are straightforward. The *S* waves impose horizontal shear tractions on horizontal planes $\tau_{xz}$ and $\tau_{yz}$ as well as the conjugate vertical planes. The rupture tip imposes horizontal shear traction parallel to the vertical fault plane $\tau_{xy}$ and the conjugate plane. These stresses interact through the shear invariant $|\boldsymbol{\tau}|$ in Eqs. 1 and 4. Here the rupture tip arrives at the base of the soil layer (Figure 3). It finds strong reverberating *S* waves already within the layer and the layer already at nonlinear failure. In this case, the shallow anelastic deformation from the *S* waves is large to that the *S* waves dominate the invariant from the rupture tip, and Eq. 6 for anti-plane fault-parallel ($y$-component) deformation from the rupture tip becomes

$$\varepsilon'_{xy,an} = \varepsilon'_0 \left[ \frac{\tau_{xy}}{|\tau|} \right] F(|\tau_{rr}|), \tag{7}$$

where index $r$ is the instantaneous resolved horizontal component of shear from the S waves. Laplace's equation in the fault parallel velocity $V_y$ solves Eq. 7 for constant $\varepsilon'_0$,

$$\left[ \frac{\partial^2 V_y}{\partial x^2} + \frac{\partial^2 V_y}{\partial z^2} \right] = 0, \tag{8}$$

where $x$ is perpendicular to the fault and $z$ is vertical. This equation can be readily solved for a boundary condition representing the base of the soil layer and a free slip boundary condition at the surface. This exercise is unnecessary here as we are not aware of a specific example of broadband recordings within meters of an earthquake fault trace. Rather, the general implication is that the horizontal and vertical scales comparable. The width of the zone of distributed slip scales with the thickness of the nonlinear soil layer.

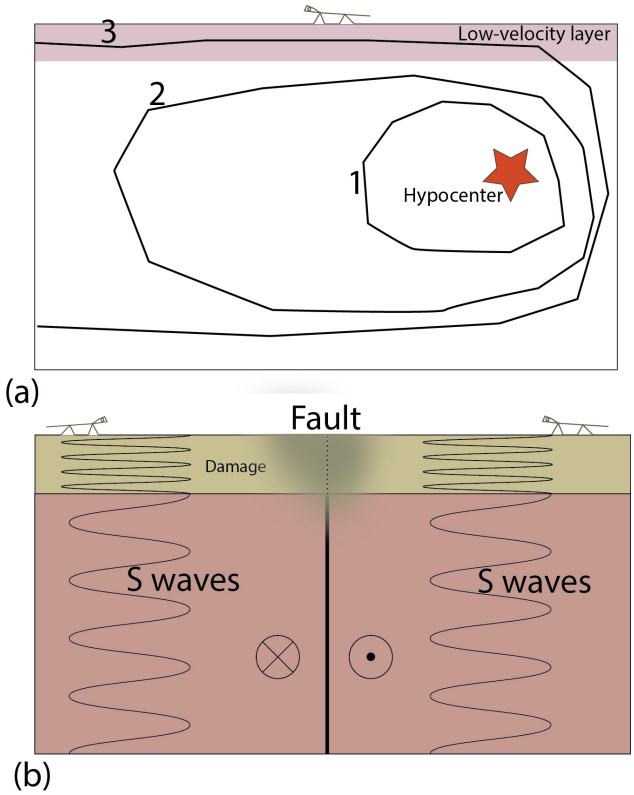


Figure 3. (a) Schematic diagram of rupture along fault plane. The rupture front (at three times) moves fast through the underlying crust but slowly through the near-surface low-velocity material. The shallow rupture front thus ascends vertically. Not to scale. (b) Schematic diagram of soil layer near fault rupture tip of strike-slip earthquake. Strong *S* waves reverberate within the soil layer bringing it into nonlinear failure. Distributed deformation occurs above the fault tip in the soil layer.

This inference yields a simple scaling relationship for the relative importance of strain rates from *S* waves and those from tectonic slip on the uppermost fault plane. We consider a

resonating *S* wave in the shallow layer. Its dynamic acceleration is

$$A = A_0 \exp\left[i(kz - \omega t)\right], \tag{9}$$

where $A_0$ has dimensions of acceleration, $z$ is depth, $t$ is time, and the wavenumber $k$ and the angular frequency $\omega$ are those of the resonating layer. That is, the thickness of the layer is dimensionally $\pi/2k$. The dynamic velocity is dimensionally $a_0/\omega$ and the strain rate from *S* waves is dimensionally $\varepsilon'_S = a_0 k/\omega = a_0/\beta$, where $\beta = \omega/k$ is the *S* wave velocity. The tectonic strain and strain rate occur laterally on both sides of the rupture tip over a distance scaling with the thickness of the resonating layer $2(\pi/2k) = \pi/k$, which nonlinear behavior from *S* waves occurs. The tectonic strain rate is thus dimensionally $\varepsilon'_{tect} = V_{slip} k/\pi$, where $V_{slip}$ slip rate on the fault during the earthquake. The ratio of *S* wave strain rate to the tectonic strain rate is thus

$$\frac{\varepsilon'_S}{\varepsilon'_{tect}} = \frac{a_0 \pi}{V_{slip} \omega}. \tag{10}$$

We provide a generic example based on the characteristics of Station KMMH16 [17]. The slip velocity of the nearby fault is 1 m/s [21] and the peak acceleration is 1 g = 10 m/s$^2$. The dominant resonating frequency is ~5 Hz. The computed ratio in Eq. 10 is ~1, indicative that the tectonic strain rate is comparable to the anelastic strain rate from *S* waves.

The gross implication that the uppermost rupture tip should interact with *S* waves carries through to this more realistic case. Nonlinear code is available to examine the process in cross section or fully in three dimensions [1-2], but onerous. The effects of strong *P* waves could be included in the model. The resonance frequency and thickness of the shallow soil near the fault trace are measurable after the earthquake. It is also possible to trench the fault trace to look for distributed anelastic deformation near the rupture. The exercise is valuable for demonstrating the reality of nonlinear rheology involving $|\tau|$. For completeness, anelastic strains from the rupture tip weaken the soil and enhance nonlinear attenuation of the *S* waves. The reverberating *S* waves should be weaker above the zone of distributed deformation that immediately to its sides. We are not aware of any suitable seismic record. We do not advocate building structures that straddle active faults to take advantage of this effect.

## Conclusions

Flow laws are an attractive rheology for modeling anelastic strain in the shallow subsurface during strong seismic shaking. In scalars, the anelastic strain rate increases nonlinearly with deviatoric stress and the deviatoric stress depends on the difference between total strain and anelastic strain. This formalism has the intuitive testable features that anelastic strain rate continues when a material is maintained at constant stress. Nonlinear attenuation of strong seismic waves depends on the anelastic strain rate. Three-dimension numerical codes exist [1-2].

Flow laws for frictional rheology provide simple scaling relations. In particular, the *S* wave acceleration in g's clips at the effective coefficient of friction. Long-lasting signal from a major event should repeatedly reach this threshold if strong *P* waves and surface waves are not present. Methods for predicting duration of shaking are available [22]. Overall, other wave types tend to

suppress high-frequency *S* waves. Still, it would be foolhardy to design a structure on the premise that other strong seismic waves will show up at just the right time to suppress *S* waves. Another practical implication is the weight of overlying structures matters when the frictional rheology depends on confining pressure [23].

Nonlinear interaction of different types of seismic waves provides natural rheological experiments. We considered two examples. (1) Confining pressure is not expected to have strong effects on shallow viscous muddy soil. Strong tensional *P* waves then to not suppress *S* waves. The dynamic horizontal acceleration can exceed 1 g, as the anelastic strain rate depends mildly nonlinearly on dynamic shear tractions. A practical application is that observed very high reverberating accelerations above muddy soil layers are not harbingers of extreme accelerations at frictional soil and rock sites. (2) Strong reverberating *S* waves bring a soil layer above a fault rupture into nonlinear failure. The anelastic strain from *S* waves interacts with that driven by fault slip to produce a distributed zone of shallow tectonic slip.

## Acknowledgments

Johanna Nevitt pointed out the mechanical problem of distributed shallow fault rupture. This research was supported by the Southern California Earthquake Center. SCEC is funded by NSF Cooperative Agreement EAR-0106924 and USGS Cooperative Agreement 02HQAG0008. The SCEC contribution number for this paper is XXXX. KiK-net data are provided by National Research Institute for Earth Science and Disaster Resilience in Japan.

## References

1. Roten D, Olsen KB, Day S, Cui Y, Fäh D. Expected seismic shaking in Los Angeles reduced by San Andreas Fault zone plasticity, *Geophysical Research Letters* 2014: **41**(8); 2769–2777.
2. Roten D, Cui Y, Olsen KB, Day SM, Withers K, Savran WH, Wang P, Mu D. High-Frequency Nonlinear Earthquake Simulations on Petascale Heterogeneous Supercomputers. *SC '16: Proceedings of the International Conference for High Performance Computing, Networking, Storage And Analysis*, 2016; pp. 957-968, IEEE Computation Society, Salt Lake City.
3. Santisi d'Avila MP, Lenti L, Semblat J-F. Modeling strong ground motion: three-dimensional loading versus wavefield polarization, *Geophysical Journal International* 2012; **90**(3), 1607-1624.
4. Hartzell SH, Bonilla LF, Williams RA. Prediction of nonlinear soil effects, *Bulletin of the Seismological Society of America* 2004; **94**(5), 1609–1629.
5. Kausel E. Assimaki D. Seismic simulation of inelastic soils via frequency-dependent moduli and damping. *Journal of Eng. Mechanics* 2002; **128**(1), 34-47.
6. Drucker DC, Prager W. Soil mechanics and plastic analysis for limit design, *Quarterly of Applied Mathematics* 1952; **10(2)**, 157–165.
7. Dieterich JH. Modeling of rock friction: 1. Experimental results and constitutive equations, *Journal of Geophysical Research* 1979; **84**(B5), 2161-2168.
8. Ruina A. Slip instability and state variable laws, *Journal of Geophysical Res*earch 1983; **88**(B12), 10,359-10,370.
9. Sleep NH, Nakata N. Nonlinear attenuation from the interaction between different types of seismic waves and interaction of seismic waves with shallow ambient tectonic stress, *Geochemistry Geophysics Geosystems* 2015; **16**(7), 2336–2363.
10. Sleep NH, Nakata N. Nonlinear Suppression of High–Frequency *S* Waves by Strong Rayleigh Waves. *Bulletin of the Seismological Society of America* 2016;**106**(5), 2302-2312.
11. Sleep NH, and Nakata N. Nonlinear attenuation of *S* waves by frictional failure at shallow depths. *Bulletin of*

*the Seismological Society of America* 2017; **107**(4), 1828–1848.
12. Aoi S., Kunugi T, Fujiwara H. Trampoline effect in extreme ground motions. *Science* 2008; **332**(5902), 727-730.
13. Yamada M, Mori J, Heaton T. The slapdown phase in high-acceleration records of large earthquakes. *Seismological Research Letters*, 2009; **80**(4), 559-564.
14. Tobita T, Iai S, Iwata T. Numerical analysis of near-field asymmetric vertical motion. *Bulletin of the Seismological Society of America*, 2010; **100**(4), 1456–1469.
15. Kinoshita S. A Stochastic Approach for Evaluating the Nonlinear Dynamics of Vertical Motion Recorded at the IWTH25 Site for the 2008$M_w$ 6.9 Iwate–Miyagi Inland Earthquake. *Bulletin of the Seismological Society of America*, 2011; **101**, 2955-2966.
16. Bradley BA, Cubrinovski M. Near-source ground motions observed in the 22 February 2011 Christchurch earthquake. *Seismological Research Letters* 2011; **82**(6), 853-865.
17. Goto H, Hata Y, Yoshimi M, Yoshida N. Nonlinear Site Response at KiK-net KMMH16 (Mashiki) and Heavily Damaged Sites during the 2016 $M_w$ 7.1 Kumamoto Earthquake, Japan. *Bulletin of the Seismological Society of America* 2017; **107**(4), 1802–1816.
18. Evans JP, Bradbury KK. Fractured dirt: Deformation textures and processes in sediment and other unconsolidated deposits. *Geology* 2007; **35**(7), 671–672.
19. Shirahama, Y, and 12 others. Characteristics of the surface ruptures associated with the 2016 Kumamoto earthquake sequence, central Kyushu, Japan. *Earth Planets Space* 2016; **68**, 191.
20. Sugito, N., Goto H, Kumahara Y, Tsutsumi H, Nakata T, Kagohara K, Matsuta N, Yoshida H. Surface fault ruptures associated with the 14 April foreshock (Mj 6.5) of the 2016 Kumamoto earthquake sequence. southwest Japan. *Earth Planets Space* 2016; **68**, 170.
21. Asano K, Iwata T. (2016) Source rupture processes of the foreshock and mainshock in the 2016 Kumamoto earthquake sequence estimated from the kinematic waveform inversion of strong motion data. *Earth, Planets Space* 2016; **68**, 147.
22. Afshari K, Stewart JP. Physically Parameterized Prediction Equations for Significant Duration in Active Crustal Regions. *Earthquake Spectra* 2016; **32**,(4), 2057-2081.
23. Petrovic B, Parolai S. Joint deconvolution of building and downhole strong-motion recordings: Evidence for the seismic wavefield being radiated back into the shallow geological layers. *Bulletin of the Seismological Society of America* 2016; **106**(4), 1720-1732.